Geophys. J. Int. (2002) **150,** 23–36

A Maslov-propagator seismogram for weakly anisotropic media

Georg Rümpker[1] and J.-Michael Kendall[2]

[1] *GeoForschungsZentrum Potsdam, Telegrafenberg,* 14473 *Potsdam, Germany. E-mail: rumpker@gfz-potsdam.de*
[2] *School of Earth Sciences, University of Leeds, Leeds, England, United Kingdom*

Accepted 2002 January 10. Received 2002 January 10; in original form 2001 June 14

SUMMARY

We introduce a formalism to calculate shear-wave seismograms for weakly-anisotropic and inhomogeneous media. The method is based on the combination of the forward-propagator method, which accounts for shear-wave interaction along a single reference ray, and the Maslov ray-summation, which incorporates amplitude and phase information from neighbouring rays to account for waveform and diffraction effects at caustics and in shadow regions. The approach is based on the assumption that the multiply split shear waves, on the way to a given receiver, travel along a common ray path that can by obtained from ray tracing in an isotropic reference medium (i.e. the common-ray approximation). The forward propagator and the Maslov amplitude are expressed with respect to radial and transverse coordinates (perpendicular to the ray propagation direction) that are defined uniquely by the initial conditions. Local polarizations and slownesses of the fast and slow shear-waves in the direction of propagation are obtained from the eikonal equation. The Maslov-propagator phase is given by the average shear-wave traveltime along the reference ray. Phase advances and delays of individual shear wave components are accounted for by the propagator. The geometrical-spreading information required for the Maslov integration is supplied by dynamic ray tracing in the isotropic reference medium. In the high-frequency limit effective phase functions are defined to assess the validity of the Maslov propagator phase information. For a homogeneous isotropic reference medium, we find good agreement with exact Maslov phase functions for anisotropic perturbations of up to 20 per cent. As a numerical application we consider effects of inhomogeneous anisotropy in a shear-wave cross-hole survey. The variations of the transversely-isotropic medium require 2-D slowness integrals. The method can handle discontinuities of the fast polarization along the ray path and also for neighbouring rays which is important for the slowness integration. Smooth transitions between isotropic and anisotropic regions along the ray path can be accounted for without the need to switch between numerical formulations.

Key words: anisotropy, Maslov seismogram, propagator methods, shear waves.

1 INTRODUCTION

While most regions of the solid Earth appear to be anisotropic, the magnitude of anisotropy rarely exceeds more than 3–4 per cent, especially in the deep Earth. Shear-wave splitting provides a good diagnostic of anisotropy, but in an inhomogeneous medium it can be quite difficult to interpret the nature of the anisotropy, especially when it is weak. For example, complications such as multipathing and shear-wave coupling make it difficult to isolate the fast and slow shear-waves. Forward modelling provides a means for interpreting such waveform complexities. Here we present a ray-based method for modelling frequency-dependent shear-wave effects in media which exhibit regions of inhomogeneous anisotropy.

The application of conventional ray-theoretical methods to anisotropic media is based on the assumption that there are two distinct shear waves that can be considered to propagate independently (Babič 1994; Červený 1972). Complications arise, for example, at finite frequencies in weakly-anisotropic media, or near slowness–surface singularities (e.g. Crampin & Yedlin 1981), where the two wavespeeds coincide. While shear-wave polarizations and raypaths can still be determined from the eikonal equation—either by numerical means or by using degenerate perturbation theory (Landau & Lifshitz 1977; Jech & Pšenčík 1989), ray-amplitude calculations in terms of the geometrical-spreading equations break down. The expressions contain terms for which the denominator is given by the velocity difference between the shear waves (e.g. Gajewski & Pšenčik 1990). A related effect arises in strongly inhomogeneous media, where the shear-wave polarizations vary rapidly along the ray path. Physically, these problems are rooted in the fact that variations in anisotropy cause frequency-dependent energy transfer (coupling) between the shear waves, which is not accounted for in the usual asymptotic approximations.

A few methods have been proposed to overcome the limitations of ray theory with respect to shear-wave coupling in weakly anisotropic media. The coupling theory of Coates & Chapman (1990) is based on a representation theorem for the displacement, where the contributions due to scattering are expressed in terms of a volume integral. The integral is simplified using the common-ray approximation to the raypaths of the shear waves. The paraxial approximation (Farra & Madriaga 1987) is then used to calculate approximate traveltimes for rays in the neighbourhood of the common (reference) ray. Rays are traced through an isotropic reference medium and shear-wave polarizations and traveltime differences are calculated using degenerate perturbation theory (Jech & Pšenčík 1989). Thomson *et al.* (1992) consider isotropic/anisotropic transition regions where the coupling is highly localized and the interference effects can be described in terms of analytical expressions. Similar connection formulae were also derived by Chapman & Shearer (1989) to describe the coupling of Snell waves near intersection and kiss singularities in depth-dependent media. Other generalizations of ray theory are referred to as quasi-degenerate and quasi-isotropic approximations (e.g. Kravtsov & Orlov 1990). Here, a solution to the wave equation is sought in terms of a linear combination of asymptotic ray theory solutions. This ansatz leads to a system of two coupled transport equations for the shear wave amplitudes. Generalizations to the elastodynamic case have been presented by several authors (e.g. Zillmer *et al.* 1998; Pšenčík 1998). The resulting seismogram is equivalent to the coupling ray theory of Coates & Chapman (1990) (for details see Zillmer *et al.* 1998). Vavryčuk (1999) has demonstrated that higher-order ray theoretical expansions can also account for shear wave coupling effects. However, how this method can be extended to wave propagation in 3-D media is not yet obvious.

Recently, Rümpker & Silver (1998, 2000) have devised a forward-propagator method to account for successive effects of shear-wave splitting along reference rays in 3-D weakly-anisotropic media. It was shown that the resulting shear-wave seismogram, again, is equivalent to the coupling ray theory of Coates & Chapman (1990) under the assumption of smoothly-varying anisotropy. The method was used to define shear-wave splitting parameters for 3-D media, which can be compared with observations of (teleseismic) shear-wave splitting. The forward propagator is expressed in terms of ray-centred coordinates given by the initial polarization of the incident reference ray and by the ray-propagation direction. We will see later that an alternative formulation in terms of fast and slow polarization directions is impracticable when it comes to the application of ray-summation methods.

Asymptotic ray theory, which forms the basis for the above mentioned methods, provides traveltimes and (limited) information on amplitude variations due to geometrical spreading. However, low-frequency diffraction effects due to the interference of rays and rapid changes in wave front curvature are not accounted for Chapman & Drummond (1982). This limitation inhibits the direct application of the ray method at, for example, caustics and in shadow regions. Ray-summation techniques, such as the WKBJ (Chapman 1978), Gaussian beam (Červený *et al.* 1982) and Maslov (Chapman & Drummond 1982) methods provide the necessary generalizations. The application of the Maslov method to high-frequency wave propagation in anisotropic media is well established (Kendall & Thomson 1993), and it provides the basis for our present approach. In anisotropic media, wave front singularities such as cusps and swallowtails are common—even (for shear waves) in homogeneous media. Ray summation methods are required to account for the corresponding waveform distortions.

We also note that, in principle, any ray-theoretical limitations regarding the solution of the wave equation can be overcome by using a direct numerical approach to solve the full hyperbolic wave-equation (e.g. Rümpker & Ryberg 2000). For 3-D media, however, computing-time and memory requirements are still beyond the possibilities of current desktop computers, thus making the application of the method as an interpretational tool impracticable. Furthermore, the completeness of numerically calculated wavefield can obscure the relation between seismogram features and model parameterization. Such practical considerations may provide further motivation for the application of more general ray-based methods. Alternatively, methods based on the factorization of the anisotropic wave equation may be used to improve computational efficiency (Thomson 1999).

In this paper we will briefly review the forward-propagator technique and give a short description of the Maslov method. Then the two methods are combined to form the Maslov propagator seismogram. The advantage of this approach lies in its ease of implementation and the fact that the time limiting step in these calculations is ray tracing in 3-D isotropic media. To illustrate its application we consider a cross-borehole shear wave survey within an inhomogeneous anisotropic section of the crust. Additional numerical examples dealing with the application of the method to wave propagation in the deep mantle will be discussed in a forthcoming paper.

2 THEORY

2.1 Forward-propagator seismogram

The derivation of the forward-propagator seismogram by Rümpker & Silver (1998, 2000) is based on the successive application of splitting operators for locally homogeneous segments along a reference ray in the anisotropic medium. Here, we summarize the results relevant to our present discussion. In the following, the displacement $\mathbf{u}$ is expressed with respect to the ray-centred coordinate system of the reference ray which is defined by the mutually orthogonal unit vectors $(\hat{\mathbf{r}}, \hat{\mathbf{t}}, \hat{\mathbf{l}})$. We consider shear waves in a weakly anisotropic medium such that the corresponding polarizations are orthogonal to the propagation direction $\hat{\mathbf{l}}$. The displacement may thus be written in the form $\mathbf{u} = (u_r, u_t)^T$. The unit vector $\hat{\mathbf{r}}$ is given by the initial polarization of the shear wave in the isotropic reference medium. In ray-centred coordinates $\hat{\mathbf{r}}$ and $\hat{\mathbf{t}}$ do not change along the reference ray (Červený 1987). In view of teleseismic applications, we also refer to $\hat{\mathbf{r}}$ as 'radial' and to $\hat{\mathbf{t}}$ as 'transverse' directions.

In the frequency domain, the shear wave displacement can be written in the form (by generalizing eq. (4) in Rümpker & Silver 1998)

$$\mathbf{u}(\omega, l) = s(\omega)\mathbf{\Gamma}(\omega, l, l_0)\hat{\mathbf{u}}_\mathbf{0} e^{i\omega\tilde{T}(l,l_0)}, \tag{1}$$

where ω is the frequency and l is the arc length along the reference ray. The function $s(\omega)$ denotes the initial waveform (due to e.g. the source), $\hat{\mathbf{u}}_\mathbf{0}$ is a vector denoting the initial displacement at l_0 (usually the initial polarization at the source) and we assume that $\hat{\mathbf{u}}_\mathbf{0} = (1, 0)$, if not stated otherwise. The solution (1) is a generalization of asymptotic-ray-theory (ART) solutions in anisotropic media, where the shear waves are considered to propagate independently. Here, the phase is given by the average traveltime $\tilde{T}$ of the fast and slow shear waves along the reference ray in the weakly anisotropic medium. The amplitude, in terms of the forward-propagator matrix $\mathbf{\Gamma}$, depends on the corresponding polarizations and also accounts for the correct time advances and delays with respect to $\tilde{T}$. Amplitude effects due to geometrical spreading are not taken into account in

this plane wave approximation. This will be incorporated when we consider the Maslov integration. In eq. (1), we write $\mathbf{\Gamma}$ with explicit dependencies to indicate that it is calculated from local parameters along the complete ray path from l_0 to l.

To define the forward propagator and in view of the numerical calculations that follow we first express the arc length l in discretized form: $l_k = (k-1)\Delta l + \Delta l/2$ with $\Delta l = (l - l_0)/N$, where N is chosen sufficiently large such that the medium can be considered homogeneous within a ray segment $(l_k - \Delta l/2, l_k + \Delta l/2)$. Thus, the average shear wave traveltime in (1) can be expressed by the sum

$$\tilde{T}(l, l_0) = \sum_{k=1}^{N} \tilde{p}_k \Delta l, \tag{2}$$

where the average shear-wave slowness is defined by

$$\tilde{p}_k = \frac{\tilde{p}^{(s)}(l_k) + \tilde{p}^{(f)}(l_k)}{2}. \tag{3}$$

The slownesses $\tilde{p}^{(s)}$ and $\tilde{p}^{(f)}$ (where the superscripts indicate fast and slow shear waves) are taken at the position l_k in the direction of propagation ($\hat{\mathbf{l}}$). In the isotropic limit, (3) corresponds to the isotropic shear wave slowness $\bar{p}_k$. In general, however, $\tilde{p}_k \neq \bar{p}_k$. This will become obvious from the numerical examples given below.

The forward propagator is obtained by multiplication of the incremental propagators along the reference ray

$$\mathbf{\Gamma}(\omega, l, l_0) = \prod_{k=1}^{N} \mathbf{\Gamma}(\omega, l_k) = \prod_{k=1}^{N} \mathbf{\Gamma}_k, \tag{4}$$

explicitly given by

$$\mathbf{\Gamma}_k = \begin{pmatrix} \cos\theta_k - i\sin\theta_k \cos\alpha_k & -i\sin\theta_k \sin\alpha_k \\ -i\sin\theta_k \sin\alpha_k & \cos\theta_k + i\sin\theta_k \cos\alpha_k \end{pmatrix} \tag{5}$$

with

$$\theta_k = \omega \delta t_k/2, \quad \alpha_k = 2\phi_k. \tag{6}$$

In (6), δt_k denotes the incremental delay time (see below) and ϕ_k is the angular difference between the polarization of the fast shear wave, $\hat{\mathbf{f}}_k$, and the radial polarization direction, $\hat{\mathbf{r}}$.

In view of (1), we find that the first (respectively second) row of the matrix (5) describes the shear-wave splitting for a single ray segment Δl when assuming that the incident wave is polarized along $\hat{\mathbf{r}}$ (respectively $\hat{\mathbf{t}}$). In the limit $\omega \to 0$, or when the medium is locally isotropic, the incremental delay time vanishes ($\delta t_k \to 0$) and the incremental propagator reduces to the unit matrix ($\mathbf{\Gamma}_k \to \mathbf{I}$). If the polarization of the incident wave is parallel (or perpendicular) to the fast polarization, $\hat{\mathbf{f}}_k$, we have $\phi_k = 0$ ($\phi_k = \pi/2$) such that $\alpha_k = 0$ ($\alpha_k = \pi$). In this case $\mathbf{\Gamma}_k$ accounts for a time advance (delay) of $\delta t_k/2$ with respect to the average traveltime, $\tilde{T}$, such that the two shear waves are separated by δt_k.

In weakly anisotropic media, the polarizations of the fast and slow shear waves can be related to the radial and transverse unit vectors by

$$\begin{pmatrix} \hat{\mathbf{f}}_k \\ \hat{\mathbf{s}}_k \end{pmatrix} = \begin{pmatrix} \cos\phi_k & \sin\phi_k \\ -\sin\phi_k & \cos\phi_k \end{pmatrix} \begin{pmatrix} \hat{\mathbf{r}} \\ \hat{\mathbf{t}} \end{pmatrix}. \tag{7}$$

In view of the numerical calculations we note that ϕ_k may be given in the form

$$\phi_k = \tan^{-1}\left(\frac{\hat{\mathbf{f}}_k \cdot \hat{\mathbf{t}}}{\hat{\mathbf{f}}_k \cdot \hat{\mathbf{r}}} \right), \tag{8}$$

such that $\phi_k \in (-\pi, \pi)$.

In (6) the incremental delay time is defined locally by

$$\delta t_k = \left[\tilde{p}^{(s)}(l_k) - \tilde{p}^{(f)}(l_k) \right] \Delta l. \tag{9}$$

In our modelling, the slownesses and polarizations in the propagation direction, $\hat{\mathbf{l}}_k$ are obtained from the eikonal equation for the anisotropic medium (Musgrave 1970) by standard numerical methods. The polarizations $\hat{\mathbf{f}}_k$ and $\hat{\mathbf{s}}_k$ are orthogonal in the limit of weak anisotropy (Coates & Chapman 1990). Numerical tests have shown that deviations from this assumption, for the more strongly anisotropic media used in our modelling, have a negligible effect.

Expressing the forward propagator with respect to (r, t) coordinates [rather than using (f, s) coordinates] has important advantages for the numerical calculations: (i) The usual ambiguity for the direction of the fast and slow polarizations by $\pm\pi$ does not affect the evaluation of the propagator (5). This is especially useful in general anisotropic media where the fast polarization may change rapidly along the ray path and where the directional sense of $\hat{\mathbf{f}}_k$ is not obvious. (ii) Once the initial displacement is defined for the whole wave front (Appendix B), the directional sense of $\mathbf{u}$ is uniquely determined along each ray path. This is a prerequisite for the application of ray summation methods, in order to avoid spurious amplitude discontinuities in the integration (see following section). (iii) Expressions (1) and (5) remain valid in isotropic media. Thus, in complex media, where rays may traverse through various anisotropic and isotropic regions, the displacement can be calculated using one single method. Setting-up unique coordinates based on fast and slow polarization directions would not be feasible in such cases.

2.2 Classical Maslov seismogram

The formulation of the forward-propagator seismogram in the previous section applies to a single reference-ray whose traveltime and amplitude is determined using ordinary ray theory (e.g. Červený & Ravindra 1971). Ordinary or zeroth-order ray theory is only concerned with rays that satisfy Fermat's principle of stationary traveltime. Low-frequency effects due to interactions between neighbouring rays on the wave front are not considered. A further disadvantage is that ordinary ray theory breaks down for certain interesting signals such as those associated with caustics, grazing rays and head waves. Ray summation methods provide valid solutions in these situations by integrating waveform contributions from neighbouring geometrical rays. In this manner, interaction effects between rays due to sharp changes in the wave front are included in the receiver waveform. Furthermore, a valid solution at and near wave front folds or caustics and an estimation of signals into shadow regions is achieved through ray summation. Here we employ the Maslov method (Maslov 1965), a ray summation approach valid for inhomogeneous media. More detail of the method can be found in Chapman & Drummond (1982), Kendall & Thomson (1993) and Huang *et al.* (1998).

In the frequency domain the Maslov integral may be written in the form

$$\mathbf{u}(\omega, \mathbf{x}) = s(\omega) \left(\frac{i\omega}{2\pi} \right)^{1/2} \int_{p_3} \mathbf{A}^{(\nu)}(x_1, x_2, p_3) e^{i\omega\Theta^{(\nu)}(x_1, x_2, p_3)}\, dp_3, \tag{10}$$

with superscript ν to discriminate between different wave types (e.g. f or s). The choice of slowness component for integration is somewhat situation depended. Ideally, the orientation of the integration axis should be chosen to cross-cut any wave front anomaly (Huang *et al.* 1998). As we will show in the numerical-examples section,

an integration over two slowness components will be more accurate or even necessary (see also Kendall & Thomson 1993; Rümpker & Thomson 1994). As our numerical examples are for a cross-borehole configuration, an integration over vertical slowness, p_3, is most convenient.

The amplitude may be expressed as

$$\mathbf{A}^{(\nu)}(x_1, x_2, p_3) = \hat{\mathbf{g}}^{(\nu)}(x_1, x_2, p_3) B^{(\nu)}(x_1, x_2, p_3), \tag{11}$$

where $\hat{\mathbf{g}}^{(\nu)}$ is the shear wave polarization and $B^{(\nu)}(x_1, x_2, p_3)$ is the Maslov amplitude.

At this point we note, that it becomes difficult to define the integral (10) when fast and slow shear wave are considered to propagate independently in the high-frequency limit. The relative (fast and slow) displacement amplitudes are determined by the initial polarization, for example, on incidence from an isotropic to an anisotropic region. Consider a medium with variable anisotropy such that the initial polarization for one segment of the wave front is parallel to the fast polarization, whereas it is parallel to the slow polarization for another segment. The integrant in (10) becomes discontinuous, if the integration is performed separately for the two wavetypes. In our example, this can be avoided by switching between wavetypes on integration. However, in more complex media the remedy is less obvious, which is a further indication for the need to consider fast and slow shear waves simultaneously (as in the following section).

However, we first continue by expressing the Maslov amplitude in the form

$$B^{(\nu)} = B_o (\rho D)^{-1/2} = B_o \rho^{-1/2} \left(\frac{\partial(x_1, x_2, p_3)}{\partial(T, q_1, q_2)} \right)^{-1/2}, \tag{12}$$

where B_o is an initial value of the amplitude and q_i are the ray take-off angles at the source. The partial derivatives required to evaluate the Jacobian D are obtained from the geometrical spreading equations (Kendall & Thomson 1989; Gajewski & Pšenčik 1990). The Jacobian D is proportional to the geometrical spreading in the mixed spatial-slowness domain (x_1, x_2, p_3) and can be rewritten

$$D = \left(\frac{\partial(x_1, x_2, x_3)}{\partial(T_1, q_1, q_2)} \right) \left(\frac{\partial p_3}{\partial x_3} \right) = J \left(\frac{\partial p_3}{\partial x_3} \right), \tag{13}$$

where J is the more conventional Jacobian used in ordinary ray theory to calculate geometrical spreading in the spatial domain, (x_1, x_2, x_3). This formulation reveals why the Maslov amplitude is valid at caustics, while the geometrical amplitude is singular. As a ray approaches a caustic, the Jacobian J shrinks to zero and the ray amplitude tends to infinity. In contrast, the term $\partial p_3 / \partial x_3$ goes to infinity at caustics. Thus, the product of the two terms in (13) remains non-singular.

The phase has the explicit form

$$\begin{aligned} \Theta^{(\nu)}(x_1, x_2, p_3) &= T^{(\nu)}\left(x_1, x_2, x_3^{(\nu)}\right) - p_3 x_3^{(\nu)} + p_3 x_3 \\ &= \tau^{(\nu)}\left(x_1, x_2, p_3^{(\nu)}\right) + p_3 x_3, \end{aligned} \tag{14}$$

where $x_3^{(\nu)}$ refers to the x_3-component at the ray endpoint, $T^{(\nu)}$ is the corresponding traveltime, and x_3 refers to the position at which the displacement is calculated. The term τ is related to traveltime by a partial Legendre transformation.

When a ray passes through a caustic the waveform experience a phase shift which is recorded by the KMAH index. To account for caustics the amplitude expression (11) must contain an additional term which includes a phase shift of usually $\pi/2$ at each frequency (a Hilbert transform) for each caustic. The amplitude may then be modified according to

$$\mathbf{A}^{(\nu)}(x_1, x_2, p_3) \rightarrow \mathbf{A}^{(\nu)}(x_1, x_2, p_3)\, e^{-\mathrm{i}\pi \,\mathrm{sgn}(\omega)\, \sigma(T_0, T)/2}, \tag{15}$$

where $\sigma(T_0, T)$ is the Maslov index defined by $\sigma = \sigma_{\mathrm{KMAH}} + [1 - \mathrm{sgn}(\partial x_1 / \partial p_1)]/2$ (e.g. Huang *et al.* 1998). The index σ_{KMAH} is an integer that is initially zero at T_0 and which usually increases by one for each caustic that is encountered (Chapman & Drummond 1982; Kendall & Thomson 1993).

Consequently, conventional ray tracing provides the information needed to calculate Maslov seismograms, that is, the traveltime, slowness, KMAH index, and the geometrical spreading terms for each ray. The time limiting step is the ray tracing.

2.3 Maslov-propagator seismogram

We are now in the position to generalize the forward propagator and to combine it with the ray summation approach provided by Maslov theory. In view of (1) and (11) we define a frequency-dependent Maslov amplitude according to

$$\tilde{\mathbf{A}}(\omega, x_1, x_2, \bar{p}_3) = \mathbf{\Gamma}[\omega, l(x_1, x_2, \bar{p}_3), l_0]\, \hat{\mathbf{u}}_0 \bar{B}(x_1, x_2, \bar{p}_3) \tag{16}$$

where the bar refers to properties of the isotropic reference medium: $\bar{p}_3$ is the vertical slowness and $\bar{B}$ is the corresponding Maslov amplitude of a shear ray in that medium. Again, we assume that the reference ray path is sufficiently close to the raypaths of the two shear waves in the anisotropic medium. Thus, the geometrical spreading and the Maslov index (see eqs 13 and 15) are obtained from ray tracing in the isotropic reference medium. Furthermore, in view of (14), the phase may be defined by

$$\tilde{\Theta}(x_1, x_2, \bar{p}_3) = \tilde{T}[l(x_1, x_2, \bar{x}_3), l_0] - \bar{p}_3 \bar{x}_3 + \bar{p}_3 x_3, \tag{17}$$

where $\bar{x}_3$ refers to the endpoint of the reference ray, and $\tilde{T}$ is the corresponding average shear-wave traveltime (2).

In view of (10), using the new expressions for the amplitude (16) and phase (17), the Maslov-propagator seismogram can be formulated as

$$\mathbf{u}(\omega, \mathbf{x}) = s(\omega) \left(\frac{i\omega}{2\pi} \right)^{1/2} \int_{\bar{p}_3} \tilde{\mathbf{A}}(\omega, x_1, x_2, \bar{p}_3)\, e^{i\omega \tilde{\Theta}(x_1, x_2, \bar{p}_3)}\, d\bar{p}_3, \tag{18}$$

where the integration is performed with respect to the vertical slowness of the reference ray. In (18) the forward propagator accounts for the interaction between fast and slow shear waves along the reference ray. The displacement is given in terms of radial and transverse coordinates such that, in general, the integration is performed separately for the two components.

Note that $\tilde{T}$ is related to the traveltime of the reference ray, $\bar{T}$, by

$$\tilde{T}(l, l_0) = \bar{T}(l, l_0) + \sum_{k=1}^{N} (\tilde{p}_k - \bar{p}_k) \Delta l, \tag{19}$$

where $\bar{p}_k$ is the slowness of the reference ray and $\tilde{p}_k$ is the average shear-wave slowness (3) in the direction of propagation. Once ray tracing through the isotropic reference model is completed, the relationship (19) can be used to reduce the amount of calculations necessary to construct the Maslov-propagator seismogram for different anisotropic models.

2.3.1 *Effective phase of the Maslov propagator*

Rümpker & Silver (1998) have derived a high-frequency approximation to the forward propagator for a smoothly-varying medium. Here, we substitute this approximation into (16) to define effective

phase functions which can be compared directly to the phase function (14) of the classical Maslov methods. This comparison provides a method to determine the accuracy of the forward-propagator seismogram in the high-frequency limit.

Writing the forward propagator in the general form

$$\mathbf{\Gamma}(\omega, l, l_0) = \begin{pmatrix} a & b \\ -\bar{b} & \bar{a} \end{pmatrix}, \tag{20}$$

the high-frequency approximation of $\mathbf{\Gamma}$ is given by Rümpker & Silver (1998), eqs (11) and (16)

$$\begin{aligned} a &= \cos\theta \cos\Big(\phi_l - \phi_{l_0}\Big) - i \sin\theta \cos\Big(\phi_l + \phi_{l_0}\Big) \\ b &= -\cos\theta \sin\Big(\phi_l - \phi_{l_0}\Big) - i \sin\theta \sin\Big(\phi_l + \phi_{l_0}\Big) \end{aligned} \tag{21}$$

where $\theta = \frac{\omega}{2} \int_l \delta t$ and $\int_l \delta t$ is the integrated delay time along the ray. The parameters ϕ_{l_0} and ϕ_l denote angular distances between $\hat{\mathbf{f}}$ and $\hat{\mathbf{r}}$ at the initial and final positions along the ray path. For the interpretation it is convenient to express the approximation (21) with respect to the (f, s)-coordinate system. In view of (7) we obtain

$$\mathbf{\Gamma}^{(fs)}(\omega, l, l_0) = \begin{pmatrix} e^{-i\frac{\omega}{2}\int_{l_0}^{l} \delta t(l')} & 0 \\ 0 & e^{+i\frac{\omega}{2}\int_{l_0}^{l} \delta t(l')} \end{pmatrix}. \tag{22}$$

Further inclusion of the phase (2) and replacing the integrals by sums leads to

$$\mathbf{\Gamma}^{(fs)}(\omega, l, l_0)\, e^{i\omega\tilde{T}(l,l_0)} = \begin{pmatrix} e^{i\omega\sum_k \tilde{p}_k^{(f)}\Delta l} & 0 \\ 0 & e^{i\omega\sum_k \tilde{p}_k^{(s)}\Delta l} \end{pmatrix}. \tag{23}$$

Eq. (23) represents phase functions corresponding to the fast and slow shear waves in the anisotropic medium. In view of (14) and (17), the effective phase of the Maslov propagator can now be defined by

$$\Theta_e^{(\nu)}(x_1, x_2, \bar{p}_3) = \tilde{T}^{(\nu)}[l(x_1, x_2, \bar{x}_3), l_0] - \bar{p}_3\bar{x}_3 + \bar{p}_3 x_3, \tag{24}$$

where

$$\tilde{T}^{(\nu)} = \sum_{k=1}^{N} \tilde{p}_k^{(\nu)} \Delta l \tag{25}$$

represents the traveltime of (fast or slow) shear wave along the reference ray and $\tilde{p}_k^{(\nu)}$ is the corresponding slowness (not to be confused with the average slowness $\tilde{p}_k$, eq. 3). The relative displacement amplitude of the two wavetypes is determined by the initial polarization. Considering the wavetypes independently, which is the case in the high-frequency approximation (24), may lead to problems in the formulation of the Maslov integral in complex media (see remarks following eq. 11). These problems do not occur when the complete Maslov-propagator formulation (18) is used, provided that the initial displacement for the complete wave front is uniquely defined.

With (11) and (16), we may also define an effective Maslov amplitude

$$\mathbf{A}_e^{(\nu)}(x_1, x_2, \tilde{p}_3) = \tilde{\hat{\mathbf{g}}}^{(\nu)}(x_1, x_2, \bar{p}_3)\bar{B}^{(\nu)}(x_1, x_2, \bar{p}_3), \tag{26}$$

where $\tilde{\hat{\mathbf{g}}}^{(\nu)}$ corresponds to either $\hat{\mathbf{f}}$ or $\hat{\mathbf{s}}$. The effective Maslov phase (24) can be compared with (14) to access the validity of the Maslov propagator in the high-frequency limit. Qualitatively, the two results agree if the reference ray represents a sufficient approximation to the raypaths of the fast and slow shear waves in the anisotropic medium. Consequently, the amplitudes (26) and (11) can also be expected to match. However, classical anisotropic Maslov theory breaks down at finite frequencies when the polarizations vary rapidly, or in the isotropic limit. The Maslov-propagator seismogram, on the other hand, remains valid in these situations.

3 NUMERICAL EXAMPLE: CROSS-HOLE SURVEY

As an application of the Maslov-propagator method, we consider a cross hole survey where two vertical boreholes are situated within an anisotropic region of the crust. A similar model was used by Guest & Kendall (1993) to illustrate the application of classical Maslov theory to forward modelling for controlled-source experiments. In the first example the elastic properties of the medium between the two wells are characterized by homogeneous transverse isotropy with a vertical symmetry axis. In a second example, we will consider inhomogeneous TI anisotropy where the symmetry axis is allowed to vary through out the model. The two wells are situated along the horizontal x_1 axis and are separated by a distance of 1 km; the x_3 axis corresponds to the vertical (Fig. 1). The source (well #1), located at $x_3 = 0$, is modelled as a point force initially oriented at an angle of 45° between the x_1 and x_2 axes. This orientation is chosen to excite SV and SH phases of similar amplitude and thus to maximize the visible effects of shear wave splitting. To simplify the analysis of waveform effects we assume a Gaussian pulse shape at the source with a pulse width of about 10 m. Three-component receivers in well #2 are located at depth intervals of 100 m.

For the modelling we have designed a generic TI medium with anisotropic elastic constants given by the isotropic P and S velocities and by two additional parameters that determine the strength and nature of the anisotropic velocity perturbations (see Appendix A

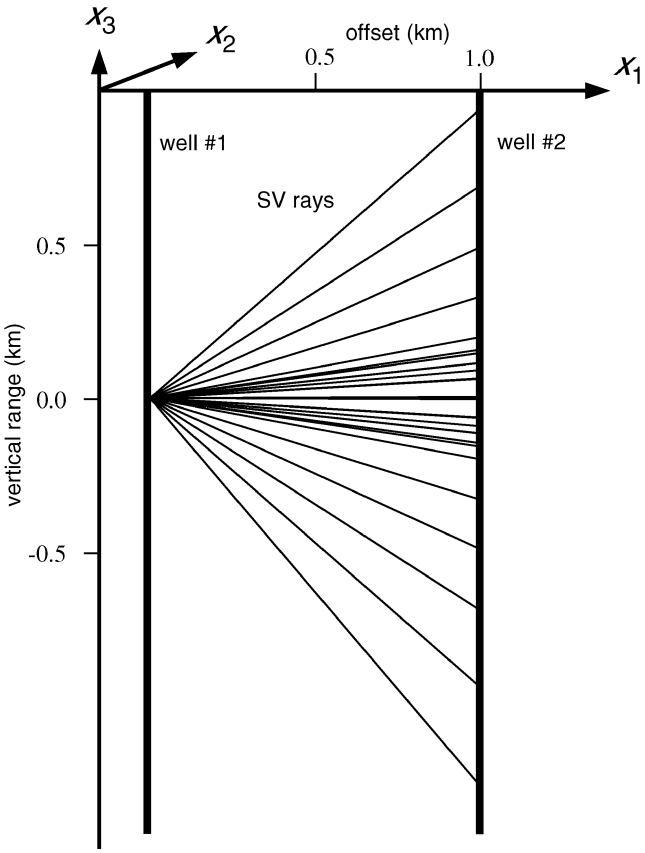

Figure 1. The locations of the two bore-holes with respect to the coordinate system.

for details). We assume a homogeneous isotropic reference medium with velocities $v_P = 4.2$ km s^{-1} and $v_S = 2.0$ km s^{-1}. To define the anisotropic perturbation we choose $a_1 = 0.2$, which corresponds to a velocity anisotropy of 20 per cent for both P and S phases. For the parameter a_0 we consider the two cases (A) $a_0 = -1$ and (B) $a_0 = +1$. It is the sign of a_0 that decides whether or not the SV slowness surface will be dimpled and the SV wave front surface will exhibit a triplication.

Fig. 2 shows sections of the slowness and wave-surfaces for the two versions of TI elastic constants. The slowness and

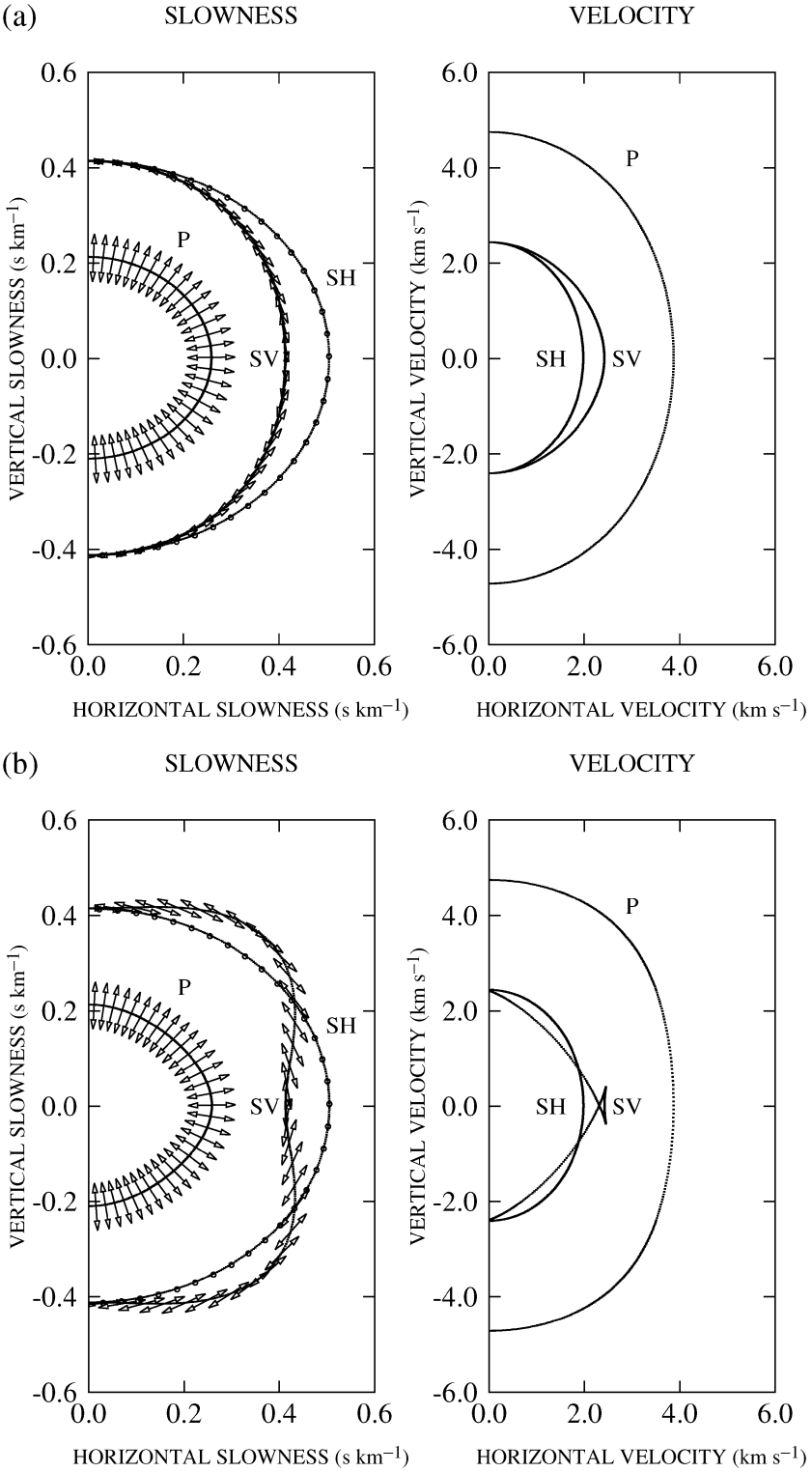

Figure 2. Vertical sections of the slowness surfaces with polarizations and the group-velocity (wave) surfaces for the homogeneous transversely-isotropic (TI) medium with a vertical symmetry axis. The medium is characterized by the two isotropic velocities $v_p = 4.3$ km s^{-1}, $v_s = 2.2$ km s^{-1} and by the anisotropy parameter $a_1 = 0.2$ which corresponds to relative (phase) velocity variations of up to 20 per cent for the two shear waves. Furthermore (a) $a_0 = -1$ and (b) $a_0 = +1$ (see Appendix A).

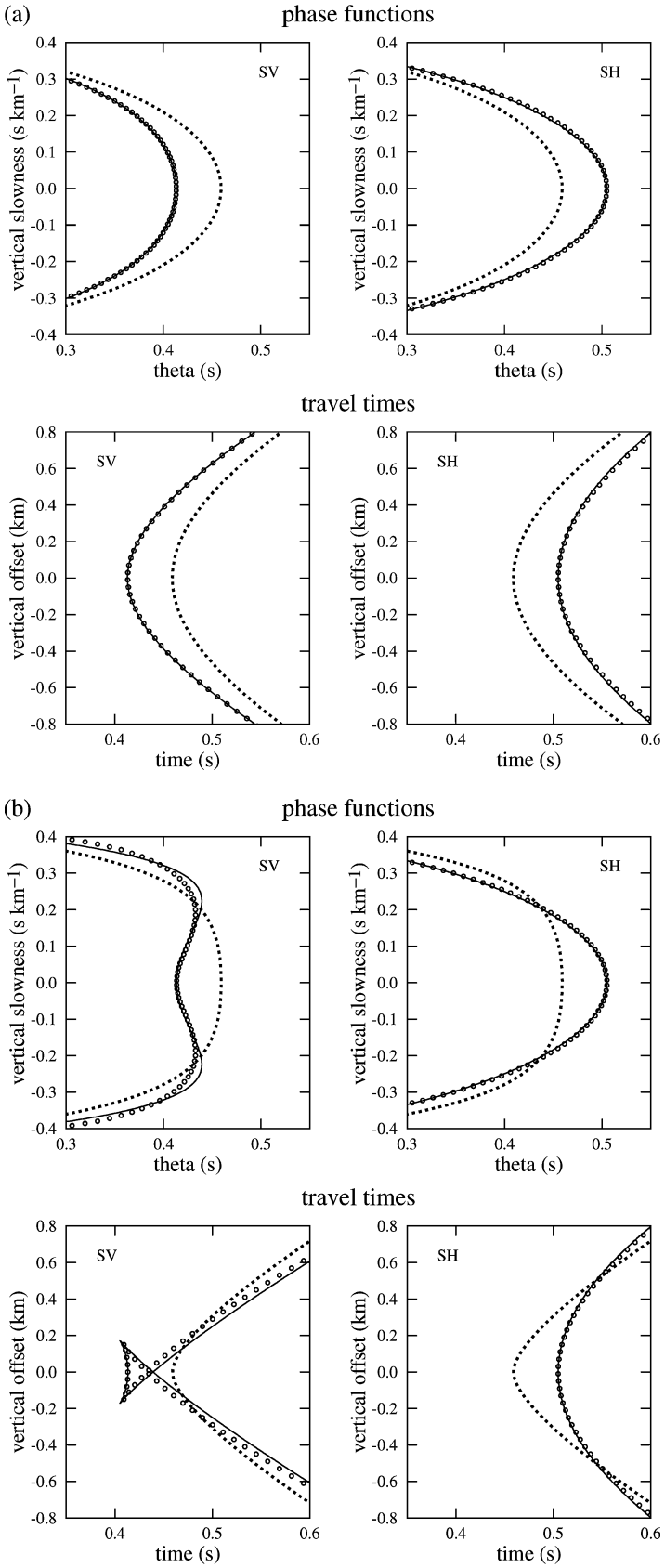

Figure 3. *SV* and *SH* phase functions as with respect to vertical slowness at receiver position $x_3 = 0$ and traveltimes as functions of receiver position. Results for the forward propagator method (solid lines) are compared with those for the classical Maslov method (circles). The dotted lines denote the average phase function of the Maslov-propagator and the corresponding traveltimes. The homogeneous TI medium between the boreholes is characterized by (a) $a_0 = -1$ and (b) $a_0 = +1$ (Fig. 2). The parameter $a_1 = 0.2$ in both cases.

group-velocity variations are shown with respect to the x_1–x_3 plane. The surfaces are rotationally invariant about the x_3 symmetry axis. For the discussion, the slowness section corresponding to a given wave type, SV or SH, can be identified from the polarizations shown in the Figure. (However, for the calculation of the Maslov propagator seismogram we require the slownesses, $\tilde{p}^{(f)}$ and $\tilde{p}^{(s)}$, in the direction $\bar{\mathbf{p}}/|\bar{\mathbf{p}}|$.) (A) The slowness sections for both, SV and SH, are concave outwards and the corresponding wavefronts are smooth (Fig. 2a). The velocity differences between SV and SH are largest for horizontally propagating waves, where SV is faster than SH. For propagation along the vertical symmetry axis the shear-wave velocities coincide at a kiss singularity. (B) With this choice of a_0 the slowness sections for SV and SH intersect and the SV-slowness curve exhibits an indentation in horizontal and vertical direction (Fig. 2b). This corresponds to a triplication of the SV wave front; the SH front remains smooth everywhere. (The triplication of the SV wave front related to the kiss singularity is vanishingly small for the current choice of a_1 and thus not obvious in Fig. 2b.) The two cases exhibit shear-wave velocity and wave front modifications which are representative of general anisotropic media. In the following we apply the Maslov-propagator method to study traveltime and waveform effects due to the different anisotropies.

3.1 Phase functions and traveltimes

In the previous section we derived effective Maslov phases, Θ_e, based on the high-frequency approximation of the forward propagator. The forward propagator and its high-frequency form are equivalent in the special case of a homogeneous medium. To assess the differences between the classical and the new formulation we compare the two phase functions, (14) and (24), for the cross-hole model. From those we can also derive traveltime curves by means of the stationary phase argument; the main contribution to the slowness integral (10) comes from points, p_3', where the derivative of $\Theta(x_1, x_2, p_3)$ with respect to p_3 vanishes. These stationary points, where $\Theta = T$ (eq. 14), correspond to geometrical arrivals (rays) at

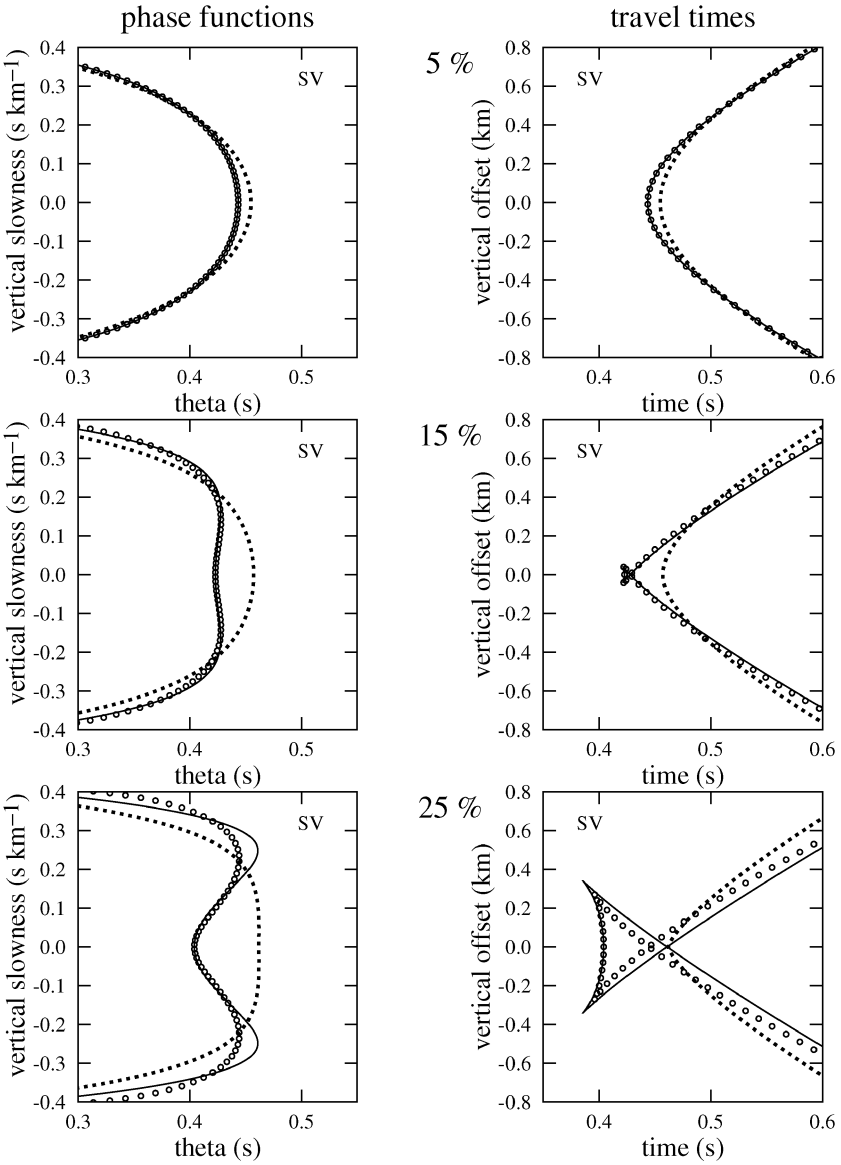

Figure 4. SV phase functions and traveltimes as in Fig. 3(b) with $a_0 = +1$. The annotations (in per cent) refer to the anisotropy parameters (top) $a_1 = 0.05$, (middle) $a_1 = 0.15$, and (bottom) $a_1 = 0.25$ chosen for the calculation.

a given receiver position (x_1, x_2, x_3) (e.g. Thomson & Chapman 1985). [The same argument applies to the high-frequency form of the Maslov propagator.]

First, we compare effective phases for the Maslov propagator (Θ_e) with those for the classical Maslov formulation (Θ). (Superscripts are used only if the discrimination between fast and slow waves is essential.) For the calculation we choose the receiver at $x_1 = 0$. Then, the stationary phase argument is applied to obtain traveltimes for a range of receiver positions. The stationary points are obtained from the numerically calculated derivative of (14) (or 23) with respect to p_3 (or $\bar{p}_3$).

Fig. 3(a) shows the two phases Θ_e and Θ for case (A) (smooth wavefronts in Fig. 2). The functions are shown with respect to the vertical slownesses $\bar{p}_3$ and p_3 respectively. In this case, the results are almost indistinguishable for both SV and SH wavetypes. Here, SV corresponds to the fast shear wave and SH to the slow shear wave, respectively. For comparison, we also show the phase, $\tilde{\Theta}$, of the Maslov-propagator seismogram (eq. 17) which corresponds to the arithmetic mean of $\Theta_e^{(s)}$ and $\Theta_e^{(f)}$. The traveltimes derived from Θ_e and from Θ agree equally well.

Fig. 3(b) shows the phase functions and corresponding traveltimes for case (B). The phases for the SV wave exhibit an indentation that relates to a triplication of the traveltime curve. Here, differences between Θ_e and Θ are somewhat more pronounced for larger values of vertical slownesses, $\bar{p}_3$ and p_3, respectively. Consequently, the size of the traveltime triplication is slightly overestimated when using Θ_e. Phase and traveltime differences are negligible for the SH wave. In view of earlier remarks (following eqs 11 and 24), we note that SV corresponds to the fast shear wave only for relatively small values of vertical slowness. For larger values, the fast shear wave is oriented SH (see Fig. 2).

The examples show the good agreement between the different phase functions and traveltimes for the cross-hole model. The differences are most pronounced for the triplicated SV wave front. In Fig. 4 phase functions and traveltimes are evaluated for three additional choices of a_1. In these examples the extent of the SV traveltime triplication strongly varies with the strength of the anisotropy. The triplication begins to occur at about $a_1 = 0.12$. Differences in traveltimes obtained from the exact and effective phase functions are assessed in Table 1. At a given receiver position we evaluated the difference $|\tilde{T} - T|$ (along corresponding segments of the traveltime curves). By varying the receiver position, we thus obtained the maximum time difference, $\max|\tilde{T} - T|$, within the displayed time window. Absolute and relative traveltime differences are given as functions of the parameter a_1. The differences remain small even for relatively strong anisotropy.

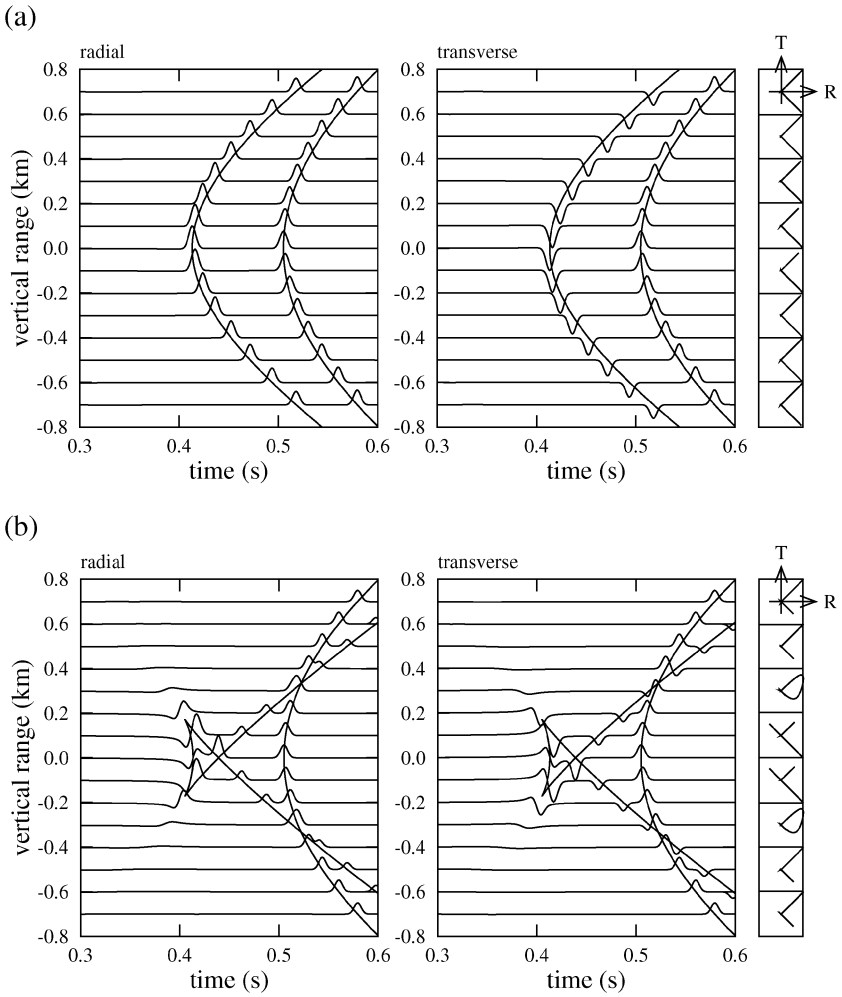

Figure 5. Maslov-propagator seismograms (1-D slowness integration) and particle motions at the receivers in well #2. The radial component corresponds to the initial polarization at the source, which is oriented at 45 degrees between SV and SH. Parameters of the medium as in Figs 2 and 3 with (a) $a_0 = -1$ and (b) $a_0 = +1$.

Table 1. Maximum values of absolute and relative traveltime differences as functions of the anisotropy parameter a_1 (Appendix A). The values at $a_1 = 5$, 15, 25 per cent have been obtained from traveltime curves for the SV phase shown in Fig. 4.

$a_1 \times 100$ per cent	$\max\lvert\tilde{T} - T\rvert$ (s)	$\frac{\max\lvert\tilde{T} - T\rvert}{T} \times 100$ per cent
2	7×10^{-5}	0.01
5	5×10^{-4}	0.1
10	2×10^{-3}	0.4
15	5×10^{-3}	1
20	0.01	2
25	0.02	4
30	0.03	6

The examples show, the Maslov propagator can account for complex wave front features, such as triplications due to curvature changes (dimples) of the slowness surface. In following we will investigate the corresponding waveform effects.

3.2 Waveforms

3.2.1 1-D slowness integration

In Fig. 5 we present waveforms calculated using the Maslov propagator for a range of receiver positions in well #2. The seismograms are shown with respect to radial and transverse coordinates (r, t), where the radial direction corresponds to the initial polarization at 45 degrees between the x_1 and x_2 axes. Thus, both, SV and SH wavetypes are excited at equal strength and appear together in the two seismogram sections. The longitudinal component (l) vanishes for shear waves in the weakly anisotropic medium. The initial waveforms are given by a Gaussian wavelet to simplify the analysis of pulse deformation effects. Eqs (16) and (17) are used to calculate the Maslov-propagator phase and amplitude. Using (13), we find that the Jacobian $D = 1$, which follows from the ray equations for a homogeneous isotropic medium. However, amplitude reduction due to geometrical spreading is still accounted for, which can be deduced from the stationary phase analysis of (18).

(A) In this case (Fig. 5a), the SV and SH wavefronts are smooth and the waveforms retain their original shape. The particle motion diagrams exhibit two distinct arrivals polarized at right angles. The time delays and advances of the wavefronts relative to the average

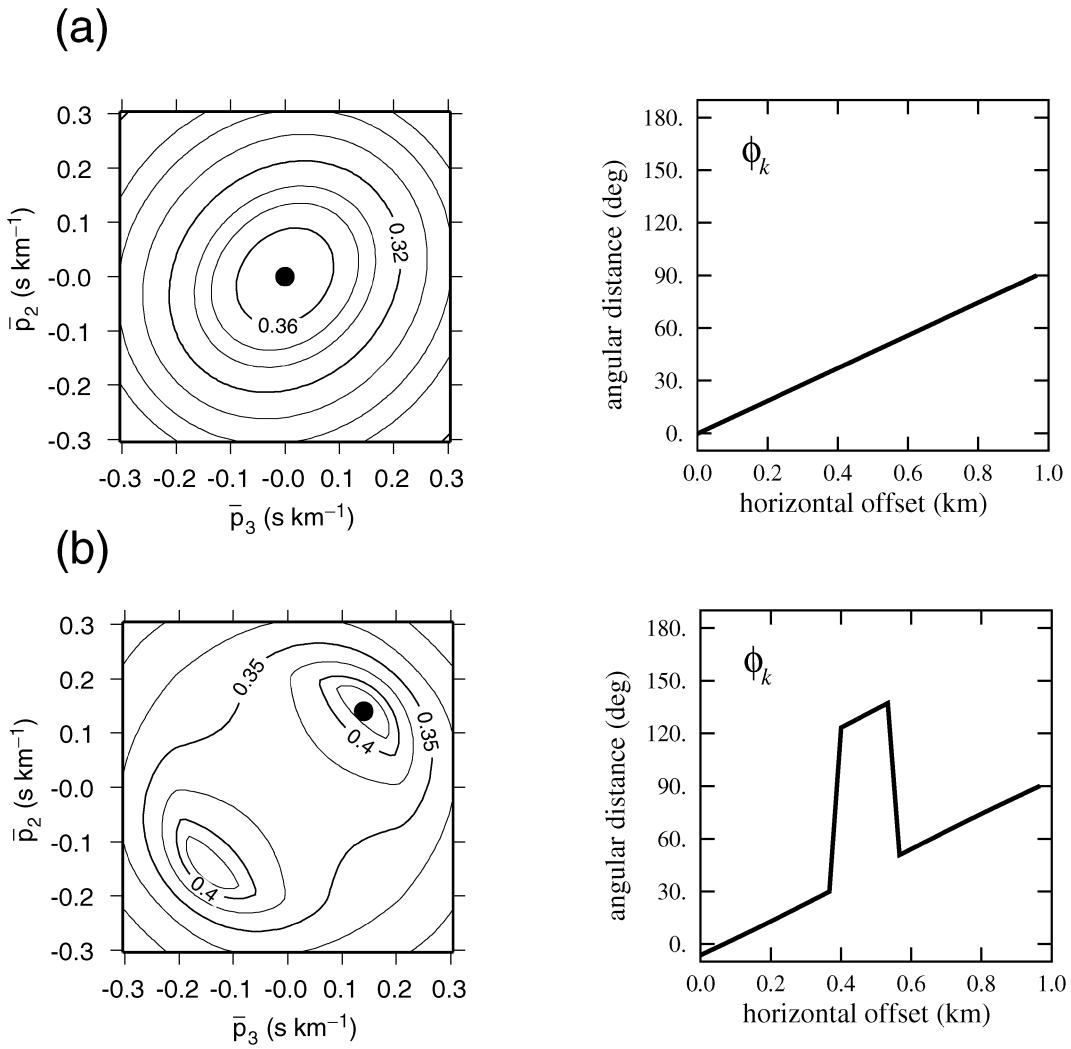

Figure 6. (Left) contours of the effective phase function $\Theta_e^{(f)}(x_1, \bar{p}_2, \bar{p}_3)$ at the receiver $(x_1, 0, 0)$ (values given in seconds). (Right) variation of angular distance between initial and fast polarization for the slowness combination (ray) marked by •. (a) $a_0 = -1$ and (b) $a_0 = +1$.

phase (17) are accounted for by the frequency-dependent forward propagator in (16). The separation between the pulses corresponds to the accumulated delay time between the holes. (B) Near the central receiver, SV components arrive first and form the wave front triplication with characteristic Hilbert-transformed pulse shapes (Fig. 5b). Low-frequency non-geometrical arrivals are related to rapid wave front-curvature changes near the cusps. The application of Maslov ray-summation is necessary to calculate the waveforms near the caustics related to the cusps, since asymptotic ray theory predicts infinitely large amplitudes here. The SH pulses are undeformed as the corresponding wave front remains smooth. The particle motion becomes elliptical at receivers where the two wavetypes overlap.

Seismograms calculated using the classical Maslov method are not shown here. The corresponding waveforms exhibit the same characteristics, except that the area affected by the wave front triplication is slightly smaller in agreement with the traveltimes shown in Fig. 3. Nevertheless, the results show that the Maslov propagator can by applied to study waveform distortions at caustics and in shadow regions.

3.2.2 2-D slowness integration

The seismograms in Fig. 5 have been obtained by 1-D integration over vertical slownesses $\bar{p}_3$. This is appropriate since, in the high-frequency limit, all contributions to the seismograms are related to rays travelling within the plane defined by the two bore-holes. Mathematically, the stationary points of the relevant phase functions, $\Theta_e(0, \bar{p}_3)$ and $\Theta_e(\bar{p}_2, \bar{p}_3)$, coincide. The situation changes if the elastic tensor is rotated with respect to the x_1-axis. After a rotation by, say, $\pi/2$, the stationary points of $\Theta_e(\bar{p}_2, \bar{p}_3)$, initially aligned vertically along $\bar{p}_3$, come to align with the horizontal $\bar{p}_2$-axis (where $\bar{p}_3 = 0$). Thus, to account for the stationary points in the case of a generally-oriented elastic tensor, 2-D slowness integration is necessary. The 2-D slowness integral with respect to $\bar{p}_2$ and $\bar{p}_3$ can be obtained by a straightforward generalization of (18) (Kendall & Thomson 1993).

In the following, we will apply the 2-D slowness integration to a laterally-varying medium with smooth variations of the symmetry axis between the wells. At well #1 we assume a horizontally oriented

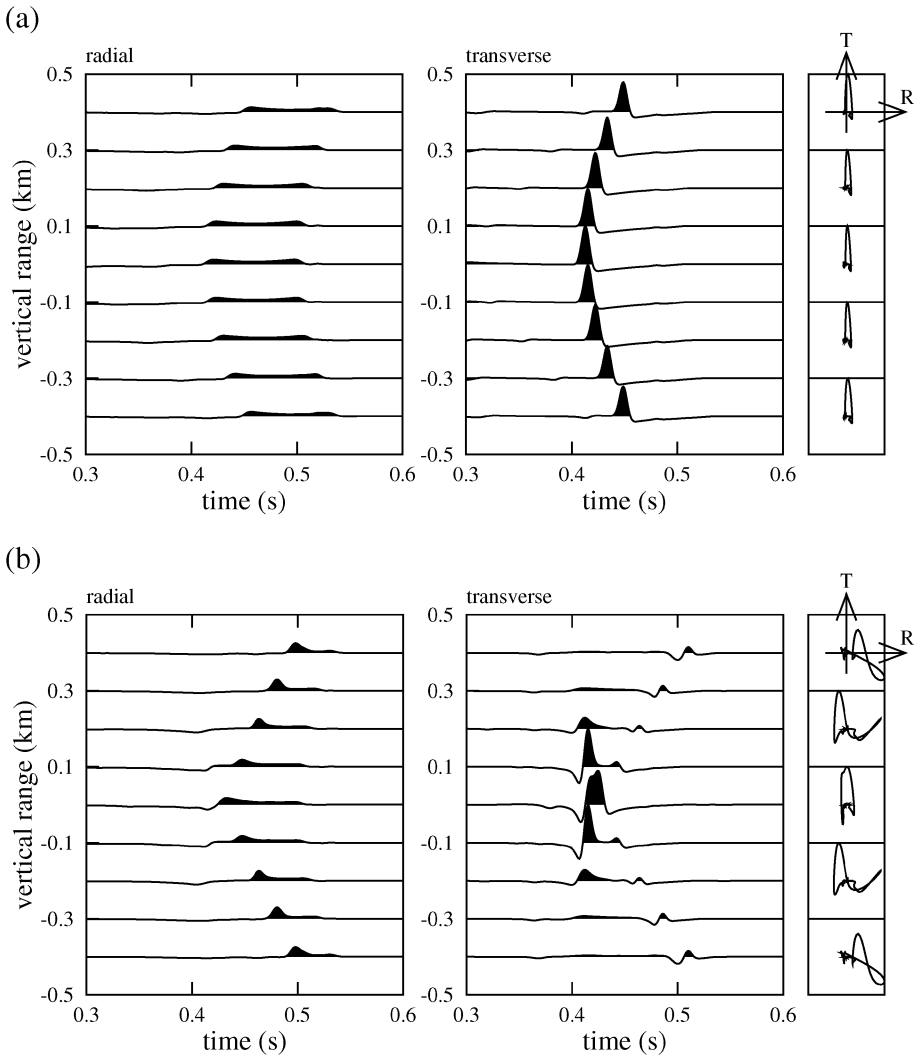

Figure 7. Maslov-propagator seismograms (2-D slowness integration) and particle motions at the receivers in well #2. The source oriented parallel to SH with a pulse width of 0.2 s. The inhomogeneous TI medium is smoothly variable and exhibits a horizontal symmetry axis at well #1 and a vertical symmetry axis at well #2. (a) $a_0 = -1$ and (b) $a_0 = +1$. The early-arriving signals of low frequency are numerical artefacts due to the finite slowness range used in the Maslov integration (see Thomson & Chapman 1986).

symmetry axis (parallel to x_2). On the way to well #2, the symmetry axis is rotated with respect to the x_1 axis by an angle $\pi/2$, according to

$$\alpha(x_1) = \pi/2(1 - x_1/1000\,\mathrm{m}),$$

such that it is oriented vertically (parallel to x_3) at well #2. For this type of medium, classical Maslov theory is no longer applicable since the shear-wave polarizations vary rapidly along the raypaths and coupling between the two wavetypes becomes important (Chapman & Shearer 1989). To illustrate this effect, we first consider the analytical solution for the displacement in the high-frequency limit, i.e. we assume that the two shear waves propagate independently within the inhomogeneous region. Using (21) and $\hat{\mathbf{u}}_\mathbf{0} = (1, 0)$, we consider two cases:

(i) $\phi_{l_0} = 0$, such that the initial polarization $\hat{\mathbf{r}}$ is parallel to the fast polarization $\hat{\mathbf{f}}$ at well #1. At the receivers (well #2), we have $\phi_l = \pi/2$ and it follows that the displacement

$$\mathbf{u} \sim e^{-i\theta}\hat{\mathbf{t}} \tag{27}$$

is purely transverse and oriented parallel to the local axis of symmetry.

(ii) For $\phi_{l_0} = \pi/2$, we note that $\hat{\mathbf{r}}$ is parallel to the slow polarization $\hat{\mathbf{s}}$ at well #1. At the receivers, $\phi_l = \pi$, and the displacement

$$\mathbf{u} \sim e^{+i\theta}\hat{\mathbf{t}} \tag{28}$$

is again purely transverse.

Thus, in the high-frequency limit, the displacement vector rotates simultaneously with the polarization vector in the medium. A specific wave type (fast or slow) excited at the source is preserved during propagation. At finite frequencies, however, the rotation of the displacement vector is incomplete and a certain amount of energy is transferred between the two wavetypes. In our example, this coupling leads to a non-zero radial displacement component at the receivers. This effect can be described using the forward propagator, whereas its high-frequency approximation and classical Maslov theory fail. For the numerical calculations given below, we have approximated the smoothly-varying anisotropic medium by a suit of 30 homogeneous layers between the wells. Numerical tests show this to be sufficient to avoid effects from discontinuous changes of material properties. Here, the source is purely SH oriented, i.e. parallel to the horizontal symmetry axis at well #1.

First, we use (24) to analyse the effective phase function $\Theta_e^{(f)}(x_1, \bar{p}_2, \bar{p}_3)$ for the fast shear wave in this medium. The result for a receiver at $x_3 = 0$ is shown in Fig. 6. For case (A) the phase exhibits a single stationary point at $\bar{p}_2 = \bar{p}_3 = 0$ which is related to a single geometrical arrival at this receiver. In addition, we show the angular distance between the initial and fast polarizations (ϕ_k, eq. 8) along the ray path: ϕ_k changes smoothly and coincides with symmetry axis in the medium. For case (B) the situation is more complicated due to three stationary points of $\Theta_e^{(f)}$ (two local maxima and a saddle point at the centre). For a geometrical arrival (ray) corresponding to one of the maxima, the angular distance, ϕ_k, varies discontinuously. It can be shown that the discontinuities are related to the variation of fast polarizations near the intersection singularities of the slowness surface (i.e. the relevant slowness sheet changes) (Fig. 2). When using the high-frequency approximation such changes along the ray path are not accounted for.

The complete Maslov-propagator seismograms (Fig. 7) are characterized by significant low-frequency radial-component energy, which is not predicted by the approximations (27) and (28). For (A), the seismograms exhibit a dominant (fast) arrival on the transverse component. In addition, on both components, a low-frequency, small amplitude signal is visible within the time-window defined by the fast and a presumed slow arrival. The latter is excited by energy leaking from the fast to the slow wave. In (B), a similar leaking effect is present, however, the seismograms exhibit up to three geometrical arrivals in correspondence with the stationary points shown in Fig. 5. Note, that at long periods, in the limit $\omega \to 0$, the transverse component vanishes, and the displacement remains radial (parallel to the initial polarization). Thus, more pronounced radial amplitudes, as indicated by the particle-motion diagrams, occur when the pulse width increases.

4 CONCLUDING REMARKS

The combination of the forward propagator and Maslov methods described in this paper allows the calculation of shear-wave seismograms in weakly-anisotropic inhomogeneous media where wavefronts are folded and traveltime curves become multivalued. Numerically, the Maslov-propagator method has the advantage that the ray path and geometrical-spreading calculations are performed for an isotropic reference medium. Anisotropic effects are accounted for in a second step, by evaluating the propagator along each reference ray. From our experience, the anisotropic slownesses and polarizations can usually be obtained from the eikonal equation by purely numerical means. Close to shear-wave singularities the analytical expressions of Jech & Pšenčík (1989) may be more appropriate. The propagator formulation in terms of radial and transverse displacement components avoids numerical problems related to the directional sense of the fast polarization. This is especially useful in media where the rays traverse through regions of rapidly changing anisotropic properties, for isotropic/anisotropic transition zones, and when it comes to the application of ray-summation methods. The propagator matrix must be evaluated separately for each discrete frequency value, which is relatively time consuming. However, the speed of the numerical calculations may be improved by using asymptotic expressions for the propagator (Rümpker & Silver 1998).

The most obvious limitation of the Maslov-propagator seismogram is related to the assumption that the raypaths of the shear waves are sufficiently close such that interference effects can be calculated along rays in an isotropic reference medium. This assumption is based on Fermats principle which shows that the effects of small (anisotropic) velocity perturbations on the traveltime between source and receiver can be accounted for, to first order, without changing the ray trajectory. Provided that this approximation holds, the Maslov-propagator method can be used with confidence (see Table 1). The common-ray approximation breaks down for shear waves in strongly inhomogeneous anisotropic media, where rays rapidly separate. However, under such 'extreme' circumstances complete numerical solutions of the wave equation might be more effective or even required.

In the numerical examples given in this paper, we kept the evaluation of the Maslov amplitude in the mixed (spatial-slowness) domain deliberately simple by choosing inhomogeneous anisotropic media for which the ray tracing was performed in a homogeneous reference medium. Examples based on a depth-dependent reference medium are discussed in a forthcoming paper, where the Maslov propagator is applied to anisotropic shear-wave propagation in global earth models. The results show that the Maslov-propagator approach remains valid for such media when the anisotropy (a_1) remains below

about 7 per cent. This value is sufficiently large to study effects of inhomogeneous anisotropy in the transition region of the mantle and at the core-mantle boundary.

ACKNOWLEDGMENTS

We would like to thank Satish Singh and an anonymous reviewer for constructive comments which helped to improve the manuscript.

REFERENCES

Babič, V.M., 1994. Ray method of calculating the intensity of wavefronts in the case of a heterogeneous, anisotropic, elastic medium, *Geophys. J. Int.,* **118,** 379–383.

Červený, V., 1972. Seismic rays and ray intensities in inhomogeneous anisotropic media, *Geophys. J. R. astr. Soc.,* **29,** 1–13.

Červený, V., 1987. Ray tracing algorithms in laterally varying layered structures, in *Seismic Tomography: with Applications in Global Seismology and Exploration Geophysics,* pp. 99–133, ed. Nolet, G., D. Reidel Publ. Co., Dordrecht.

Červený, V. & Ravindra, R., 1971. *Theory of Seismic Head Waves,*University of Toronto Press, Toronto.

Červený, V., Popov, M.M. & Pšenčík, I., 1982. Computation of wavefields in inhomogeneous media—Gaussian beam approach, *Geophys. J. R. astr. Soc.,* **70,** 109–128.

Chapman, C.H., 1978. A new method for computing synthetic seismograms, *Geophys. J. R. astr. Soc.,* **54,** 481–518.

Chapman, C.H. & Drummond, R., 1982. Body-wave seismograms in inhomogeneous media using Maslov asymptotic theory, *Bull. seism. Soc. Am.,* **72,** 277–317.

Chapman, C.H. & Shearer, P.M., 1989. Ray tracing in azimuthally anisotropic media—II. Quasi-shear wave coupling, *Geophys. J. Int.,* **96,** 65–83.

Coates, R.T. & Chapman, C.H., 1990. Quasi-shear wave coupling in weakly anisotropic 3-D media, *Geophys. J. Int.,* **103,** 301–320.

Crampin, S. & Yedlin, M., 1981. Shear-wave singularities of wave propagtion in anisotropic media, A review of wave motion in anisotropic and cracked elastic media, *J. Geophys.,* **49,** 43–46.

Gajewski, D. & Pšenčik, I., 1990. Vertical Seismic Profile Synthetics by Dynamic Ray Tracing in Laterally Varying Anisotropic Structures, *J. geophys. Res.,* **95,** 11 301–11 315.

Farra, V. & Madriaga, R., 1987. Seismic waveform modelling in heterogeneous media by ray perturbation theory, *J. geophys. Res.,* **92,** 2697–2712.

Guest, W.S. & Kendall, J.-M., 1993. Modelling seismic waveforms in anisotropic inhomogeneous media using ray and Maslov asymptotic theory: applications to exploration seismology, *Can. J. Explo. Geophys.,* **29,** 78–92.

Huang, X., Kendall, J.-M., Thomson, C.J. & West, G.F., 1998. A comparison of the Maslov integral seismogram and the finite-difference method, *Geophys. J. Int.,* **132,** 584–594.

Jech, J. & Pšenčík, 1989. First-order perturbation method for anisotropic media, *Geophys. J. Int.,* **99,** 369–376.

Kendall, J.-M. & Thomson, C.J., 1989. A comment on the form of the geometrical spreading equations, with some numerical examples of seismic ray tracing in inhomogeneous, anisotropic media, *Geophys. J. Int.,* **99,** 401–413.

Kendall, J.-M. & Thomson, C.J., 1993. Maslov ray summation, pseudocaustics, Lagrangian equivalence and transient seismic waveforms, *Geophys. J. Int.,* **113,** 186–214.

Kravtsov, Yu.A. & Orlov, Yu.I., 1990. *Geometrical Optics of Inhomogeneous Media,* Springer Verlag, Berlin.

Landau, L.D. & Lifshitz, E.M., 1977. *Quantum Mechanics—Nonrelativistic Theory,* Pergamon Press, Oxford.

Maslov, V.P., 1965. *Theory of Perturbations and Asymptotic Methods,* Izd., MGU, Moscow (in Russian).

Musgrave, M.J.P., 1970. *Crystal Acoustics,* Holden–Day, San Francisco.

Pšenčík, I., 1998. Green's function for inhomogeneous weakly anisotropic media, *Geophys. J. Int.,* **135,** 279–288.

Rümpker, G. & Ryberg, T., 2000. New 'Fresnel-zone' estimates for shear-wave splitting observations from finite-difference modelling, *Geophys. Res. Lett.,* **27,** 2005–2008.

Rümpker, G. & Silver, P.G., 1998. Apparent shear-wave splitting parameters in the presence of vertically-varying anisotropy, *Geophys. J. Int.,* **135,** 790–800.

Rümpker, G. & Silver, P.G., 2000. Calculating splitting parameters for plume-type anisotropic structures of the upper mantle, *Geophys. J. Int.,* **143,** 507–520.

Rümpker, G. & Thomson, C.J., 1994. Seismic-waveform effects of conical points in gradually varying anisotropic media, *Geophys. J. Int.,* **118,** 759–780.

Thomson, C.J., 1999. The 'gap' between seismic ray theory and 'full' wavefield extrapolation, *Geophys. J. Int.,* **137,** 364–380.

Thomson, C.J. & Chapman, C.H., 1985. An introduction to Maslov's asymptotic method, *Geophys. J. R. astr. Soc.,* **83,** 143–168.

Thomson, C.J. & Chapman, C.H., 1986. Endpoint contributions to synthetic seismograms, *Geophys. J. R. astr. Soc.,* **87,** 285–294.

Thomson, C.J., Kendall, J.-M. & Guest, W.S., 1992. Geometrical theory of shear–wave splitting: corrections to ray theory for interference in isotropic/anisotropic transitions, *Geophys. J. Int.,* **108,** 339–364.

Vavryčuk, V., 1999. Applicability of high-order ray theory for S-wave propagation in inhomogeneous weakly anisotropic media, *J. geophys. Res.,* **104,** 28 829–28 840.

Zillmer, M., Kashtan, B.M. & Gajewski, D., 1998. Quasi-isotropic approximation of ray theory for anisotropic media, *Geophys. J. Int.,* **132,** 643–653.

APPENDIX A: GENERIC TI ELASTIC CONSTANTS

The matrix of elastic constants for a general transversely isotropic medium with a vertical (x_3) axis of symmetry may be given in the form (Musgrave 1970)

$$\begin{pmatrix} C_{11} & C_{11}-2C_{66} & C_{13} & 0 & 0 & 0 \\ C_{11}-2C_{66} & C_{11} & C_{13} & 0 & 0 & 0 \\ C_{13} & C_{13} & C_{33} & 0 & 0 & 0 \\ 0 & 0 & 0 & C_{44} & 0 & 0 \\ 0 & 0 & 0 & 0 & C_{44} & 0 \\ 0 & 0 & 0 & 0 & 0 & C_{66} \end{pmatrix}. \tag{A1}$$

For our modelling, it is convenient to express the elastic constants in terms of isotropic P and S (reference) velocities. In this paper, anisotropic effects are taken into account by two parameters a_0 and a_1. The parameter a_1 determines both, the maximum variation in P-wave (phase) velocity for propagation along different axes, and the differences between fast and slow S-wave velocities in the plane perpendicular to the symmetry axis. For example, $a_1 = 0.1$ corresponds to a velocity anisotropy of 10 per cent for both P and S waves. We define the density-normalized elastic constants by

$$C_{11} = \left(v_p - \frac{a_1 v_p}{2}\right)^2, \quad C_{33} = \left(v_p + \frac{a_1 v_p}{2}\right)^2, \tag{A2a}$$

$$C_{66} = \left(v_s - \frac{a_1 v_s}{2}\right)^2, \quad C_{44} = \left(v_s + \frac{a_1 v_s}{2}\right)^2. \tag{A2b}$$

The constant C_{13} may be defined such that $C_{13} = (v_p^2 - 2v_s^2)$ in the isotropic limit ($a_1 = 0$). Here we choose

$$C_{13} = (1 + a_0 a_1)\left(v_p^2 - 2v_s^2\right), \tag{A2c}$$

where, in our examples, a_0 is either $+1$ or -1. This parameter determines the (Gaussian) curvature of the slowness and group-velocity (wave) surfaces. In this formulation of the elastic constants (A2) no assumptions have been made regarding the strength of the anisotropy. See examples given in the main part of the paper.

APPENDIX B: INITIAL CONDITIONS

The initial shear-wave slowness vector **p** is determined by the take-off angles of the reference ray at the source and the isotropic shear-wave velocity. Using the ray direction $\hat{\mathbf{l}}$ as a basis, we may define the perpendicular $\hat{\mathbf{S}}_V$ and $\hat{\mathbf{S}}_H$ polarization directions according to

$$\hat{\mathbf{l}} = \hat{\mathbf{p}}, \quad \hat{\mathbf{S}}_H = \left(\frac{-l_2}{\sqrt{l_1^2 + l_2^2}}, \frac{l_1}{\sqrt{l_1^2 + l_2^2}}, 0 \right), \quad \hat{\mathbf{S}}_V = \hat{\mathbf{l}} \times \hat{\mathbf{S}}_H, \tag{B1}$$

The initial shear-wave polarization, $\hat{\mathbf{r}}$, and its transverse, $\hat{\mathbf{t}}$, can be expressed by

$$\begin{aligned} \hat{\mathbf{r}} &= \cos\phi_r \hat{\mathbf{S}}_V + \sin\phi_r \hat{\mathbf{S}}_H \\ \hat{\mathbf{t}} &= -\sin\phi_r \hat{\mathbf{S}}_V + \cos\phi_r \hat{\mathbf{S}}_H \end{aligned}. \tag{B2}$$

In weakly anisotropic media the polarizations of the fast and slow shear-waves are also perpendicular to the ray direction $\hat{\mathbf{l}}$ and may thus be expressed according to

$$\begin{aligned} \hat{\mathbf{f}} &= \cos\phi_f \hat{\mathbf{S}}_V + \sin\phi_f \hat{\mathbf{S}}_H \\ \hat{\mathbf{s}} &= -\sin\phi_f \hat{\mathbf{S}}_V + \cos\phi_f \hat{\mathbf{S}}_H \end{aligned}. \tag{B3}$$

With the previous definitions we may employ (8) which yields the angle between the initial polarizations and the fast polarization at l_1

$$\phi_1 = \phi_f - \phi_r. \tag{B4}$$

In practice, the polarizations $\hat{\mathbf{f}}$ and $\hat{\mathbf{s}}$ are determined with respect to (x_1, x_2, x_3) coordinates using the eikonal equation. Then (B3) with (B1) are used to obtain ϕ_f. The angle ϕ_r can be chosen according the assumed (or calculated) source characteristics (see B2). For example, $\phi_r = 0$, if the source is assumed to be oriented in $\hat{\mathbf{S}}_V$ direction. More realistic source characteristics may be derived from a point-source analysis.